Room temperature structures beyond 1.5 Å by serial femtosecond crystallography

Marius Schmidt' , Kanupriya Pande, Shibom Basu, and Jason Tenboer

Citation: Structural Dynamics **2**, 041708 (2015); doi: 10.1063/1.4919903
View online: http://dx.doi.org/10.1063/1.4919903
View Table of Contents: http://aca.scitation.org/toc/sdy/2/4
Published by the American Institute of Physics

Room temperature structures beyond 1.5 Å by serial femtosecond crystallography

Marius Schmidt,[1,a)] Kanupriya Pande,[1] Shibom Basu,[2] and Jason Tenboer[1]
[1]*Physics Department, University of Wisconsin Milwaukee, Milwaukee, Wisconsin 53211, USA*
[2]*Department of Chemistry and Biochemistry, Arizona State University, Tempe, Arizona 85287, USA*

(Received 8 March 2015; accepted 28 April 2015; published online 7 May 2015; corrected 15 May 2015)

About 2.5 × 10^6 snapshots on microcrystals of photoactive yellow protein (PYP) from a recent serial femtosecond crystallographic (SFX) experiment were reanalyzed to maximum resolution. The resolution is pushed to 1.46 Å, and a PYP structural model is refined at that resolution. The result is compared to other PYP models determined at atomic resolution around 1 Å and better at the synchrotron. By comparing subtleties such as individual isotropic temperature factors and hydrogen bond lengths, we were able to assess the quality of the SFX data at that resolution. We also show that the determination of anisotropic temperature factor ellipsoids starts to become feasible with the SFX data at resolutions better than 1.5 Å.
[http://dx.doi.org/10.1063/1.4919903]

INTRODUCTION

Photoactive Yellow Protein (PYP) is a blue light receptor in purple bacteria. It has been discovered in the 1980s (Meyer, 1985) and has since generated vast interest by a large group of researchers worldwide. After absorption of a blue photon, PYP enters a photocycle with numerous intermediates that accumulate and decay on multiple time-scales from picoseconds to seconds. The progression of the photocycle is controlled by a configurational change, a *trans* to *cis* isomerization, of the central chromophore para-cinnamic acid (PCA) that is covalently linked to Cys-69 of the protein (Fig. 1). The configurational change drives conformational changes of the protein with distinct intermediates. Before the photocycle comes to an end, the chromophore relaxes back to the *trans* configuration. Over the years, the photocycle has been extensively investigated with time-resolved crystallography on time-scales from 100 ps, the pulse duration of a synchrotron X-ray pulse, to seconds, when the reaction ends (Ihee *et al.*, 2005; Jung *et al.*, 2013; Schmidt *et al.*, 2004; Schmidt *et al.*, 2013; and Schotte *et al.*, 2012). However, there is substantial interest to investigate the PYP reaction on ultrafast time-scales exploiting the femtosecond X-ray pulses at the Free Electron Lasers for hard X-rays (X-ray FELs). A proof-of-principle experiment has been recently (June 2014) performed on PYP at the Linac Coherent Light Source's (LCLS) beamline CXI using time-resolved serial femtosecond crystallography (TR-SFX) at near atomic (1.6 Å) resolution with time-delays 10 ns and 1 μs after an optical pump laser pulse (Tenboer *et al.*, 2014). The experiment shows that TR-SFX is feasible at an X-ray FEL. The door is now open to explore faster time-scales and potentially the femtosecond time-regime of the PYP photocycle. However, we anticipate that on the ultra-fast time-scale, structural changes are small and meaningful details can only be obtained if resolution is high enough. Here, we make use of the roughly 2.5 × 10^6 snapshots that were collected during the

a)Author to whom correspondence should be addressed. Electronic mail: smarius@uwm.edu

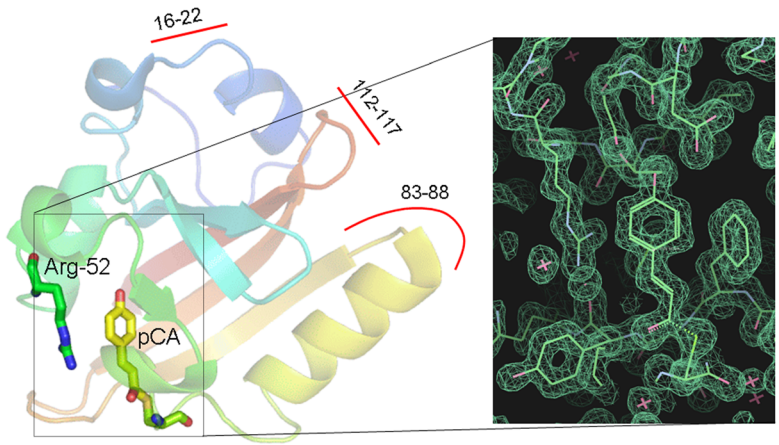

FIG. 1. Structure of PYP, ribbon representation, rainbow color distinguishes different moieties. Arg-52 and PCA chromphore are marked. Red bars mark regions with comparatively high disorder. Right panel: exemplary electron density (on the 1.3 σ level) of the chromophore region.

June 2014 experiment in the dark to extend the resolution to 1.46 Å. We refined the PYP structural models against the SFX data at this resolution, and compared sensitive parameters such as temperature (B-) factors and hydrogen bond lengths to those derived from models that were obtained from in-house X-ray sources at near atomic resolution or synchrotron X-ray sources at atomic resolution.

METHODS

Methods are published earlier (Tenboer *et al.*, 2014). In brief: PYP micro-crystals were grown from highly concentrated PYP. The crystals were about 5 μm long needles with 2 μm diameter (Fig. 2(a)). The suspension (5×10^{11} crystals/ml) was jetted into vacuum by a gas dynamic virtual nozzle (Weierstall *et al.*, 2012). FEL X-ray pulses of 40 fs duration containing about 10^{11} photons/pulse were directed on the jet about 75 μm from the nozzle exit. The temperature of the jet was not controlled. However, since the jet velocity is about 10 m/s, the 75 μm path through the vacuum of the chamber until it is intercepted by the X-rays translates to about 7.5 μs. Assuming a cooling rate of 10^6 K/s, the jet cools about 7.5 K. Hence, the temperature at the X-ray FEL beam intersection can be estimated to be about 15 °C, which is close to ambient (room) temperature. Diffraction patterns were collected by a Cornell SLAC Pixel Area Detector (CSPAD) located 75.1 mm from the jet. The center of the CSPAC was

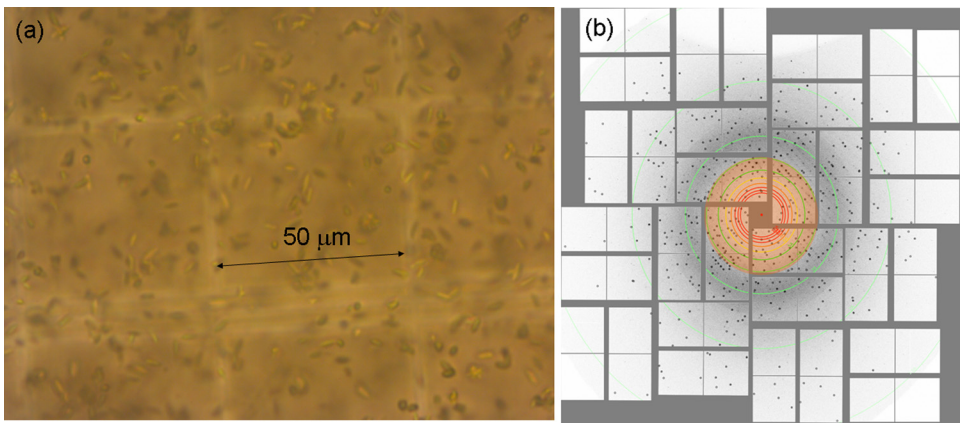

FIG. 2. (a) Microcrystals in the Neubauer counting chamber, (b) diffraction pattern on the CSPAD. The electronic attenuation mask is shown in orange.

electronically attenuated by about a factor of ∼7 to allow for an increase in the dynamic range that allows the simultaneous collection of low and high resolution reflections (Fig. 2(b)). With this setup, about 2.5×10^6 diffraction patterns (snapshots) were collected in the dark (Table I). Snapshots containing Bragg reflections were identified by CHEETAH (Barty *et al.*, 2014). Indexing and integration was done by CrystFEL (White *et al.*, 2012). The indexing ambiguity of the hexagonal PYP crystals was solved by methods (Brehm and Diederichs, 2014) implemented in CrystFEL.

Refinement was carried out with "REFMAC5" (Murshudov *et al.*, 2011) using the "log-likelihood residual." B-factors were averaged for individual amino acid residues by "MOLEMAN" (Kleywegt *et al.*, 2001) over the backbone atoms N, C_α, C, and O. These B-factors $\langle B \rangle_{ind}$ were plotted as a function of residue number. The trans/cis isomerization of the chromophore is controlled by three hydrogen bonds (Fig. 3(a)). Two extend from the phenolate oxygen (O4) of the chromophore head to O^δ of Glu-46 and O^η of Tyr-42, and the third hydrogen bond is formed by the carbonyl-oxygen of the chromophore foot and the peptide bond nitrogen of Cys-69. The lengths of the O4-O^δ and O4-O^η hydrogen bonds might depend also on the bond length of the chromophore ring C4' to the hydroxyl oxygen O4 (Fig. 3(a)), which is set to the relatively large value 1.362 Å by a restraint in the "REFMAC5" library file "mon_lib.cif." If the X-ray data are weak and low resolution, this restraint enforces short hydrogen bonds. However, we tested this by setting the restraint to 1.238 Å, which is typically found in older "CNS" (Brunger *et al.*, 1998) and "XPLOR" (Brunger *et al.*, 1990) parameter files. This should bias the refinement towards longer hydrogen bonds. Refinement was carried out with either restraints (see below). The lengths of the hydrogen bonds were measured by the program "COOT" (Emsley *et al.*, 2010) and compared to those found within existing structures in the literature.

RESULTS

The SFX data were integrated to a resolution of 1.37 Å. However, the R_{split} is unacceptable (84.3%) at this resolution, and it is difficult to use it to determine a resolution limit. The I/sigI (Table I) which is frequently used in crystallography to determine the resolution limit is differently determined in SFX due to the lack of profile fitting, the large shot-to-shot intensity variations as well as spectral fluctuations of the FEL X-ray beam (Karplus and Diederichs, 2012; White, 2014; and White *et al.*, 2012). In order to estimate that limit, we used Fourier Shell Correlation (FSC), Eq. (1), which is output by REFMAC5 (Brown *et al.*, 2015). The FSC is routinely employed in electron microscopy where it is the "gold-standard" to estimate the resolution limit (Scheres, 2012). The FSC was calculated to 1.37 Å in 25 resolution bins (Eq. (1)) and plotted as a function of $4 \sin^2\theta/\lambda^2 = \frac{1}{d^2}$, where d is the resolution

$$FSC = \frac{\sum_h |F^{obs}||F^{calc}|}{\sqrt{\sum_h |F^{obs}|^2} \sqrt{\sum_h |F^{calc}|^2}}. \quad (1)$$

TABLE I. Data collection statistics (last resolution shell: 1.49–1.46 Å).

Diffraction pattern	2 463 000
Hits	170 853 (7% of total)
Indexed	118 260 (69% of hits, 4.8% of total)
Resolution	1.46 Å
# unique reflections	16787
Competeness [%]	100
I/sigI	9.0 (0.3)
R_{split} (%)	6.89 (56.7)

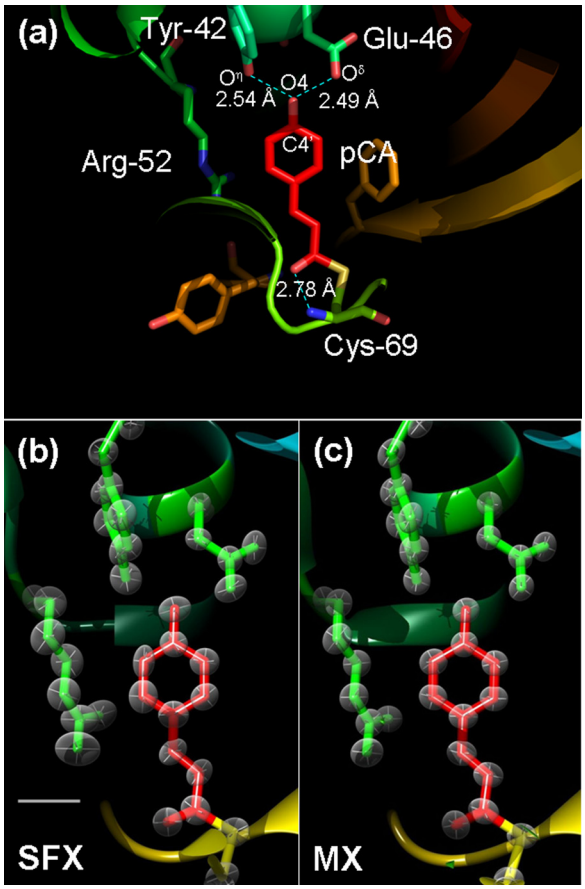

FIG. 3. The chromophore pocket in PYP. (a) Hydrogen bonds marked by blue dashed lines; the pCA chromophore, Tyr-42, Glu-46, and Cys-69 are marked. Distances found in the refined PYP_{SFX} structure are indicated. (b) Chromophore pocket residues with thermal ellipsoids (gray) from anisotropic individual B-factor refinement against the SFX data at 1.46 Å resolution, (c) thermal ellipsoids from cryo-crystallography at 0.82 Å resolution. The ellipsoids are 2-fold enlarged for clarity. The gray bar in (b) denotes an average displacement, $\langle \Delta x \rangle$, of about 1 Å. (a) produced by PYMOL (DeLano, 2006), and (b) and (c) by CHIMERA (Pettersen *et al.*, 2004).

To evaluate the resolution limit, we refined a PYP model with increasing resolution limits and stopped increasing the resolution when the FSC between the observed SFX amplitudes ($|F^{obs}|$) and those calculated from the model ($|F^{calc}|$) falls below 50%, which happened at 1.46 Å (Fig. 4). For the refinement, we started with the original PYP model (Borgstahl *et al.*, 1995) with PDB (Berman *et al.*, 2002)-entry 2PHY. We removed the double conformations in 2PHY and the water molecules. After rigid-body and restrained refinement, water molecules were added and double conformations were identified using Fo-Fc difference electron density maps. The refinement settles at 16.5% R_{cryst} and 20.1% R_{free} (Table II). The average B-factor is 13.5 $Å^2$. Anisotropic B-factor refinement decreases the R-factors further to 11.9% and 18.1%, respectively (Table II). Isotropic temperature factors averaged over the backbone atoms, $\langle B \rangle_{ind}$, are shown in Fig. 5(a) (black line). Hydrogen bond distances of the chromophore head to Glu-46 and Tyr-42 are 2.54 Å and 2.49 Å, respectively (Table II).

DISCUSSION

The number of unique reflections at 1.46 Å (16787, Table I) determined from the $\sim 2.5 \times 10^6$ SFX snapshots enables the refinement of an anisotropic B-factor model. The

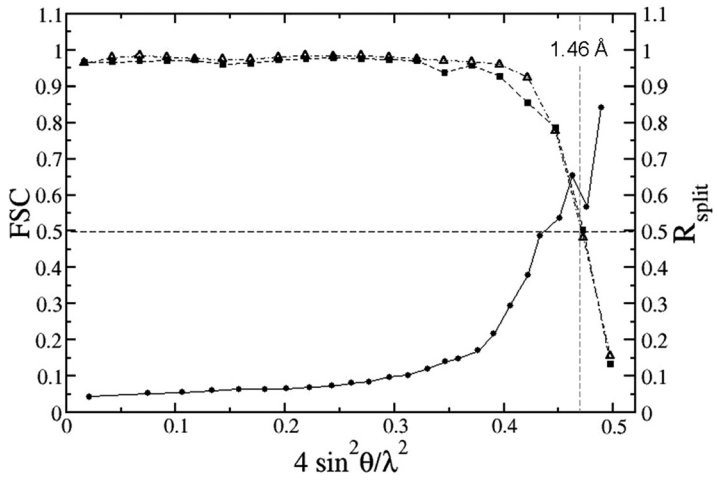

FIG. 4. Fourier Shell Correlation and R_{split} as function of $1/d^2$ (d is resolution). Open triangles and dashed-dotted line: FSC_{work}, solid squares and dashed line: FSC_{free}, solid line and spheres: R_{split}. Vertical long dashed line: 1.46 Å resolution.

resulting thermal ellipsoids are shown in Fig. 3(b). Notably, R_{cryst} and R_{free} factors decrease substantially. Obviously, the PYP structural model that includes anisotropic temperature factor ellipsoids is superior to the one with only isotropic B-factors. In Fig. 3(c), the thermal ellipsoids from a PYP structure refined to 0.82 Å with conventional macromolecular crystallographic (MX) data at cryogenic temperatures are shown (for the model see below, and Table II). The ellipsoids hardly differ regardless whether SFX or ultra-high resolution data are used. This is an indication that SFX provides adequate data for such a refinement. The gap between R_{cryst} and

TABLE II. Refinement statistics, B-factors, and hydrogen bond lengths. H1: PCA-phenolate oxygen to Glu-42 O^{δ}. H2: PCA-phenolate O to Tyr-42 O^{η}, H3: PCA-carbonyl O^{1} to Cys-69 N. All studies were performed on hexagonal $P6_3$ wt-PYP crystals with unit cell parameters (depending on temperature) around a = b = 66 Å, c = 40 Å.

pdb	PYP_{SFX} this study	PYP_{B293} 2PHY	PYP_{A293} 1OTB	PYP_{A110} 1OT9	PYP_{G149} INWZ
X-ray source	LCLS	rotating anode	APS	APS	SSRL
Method	SFX	rotation	rotation	rotation	rotation
Crystal size	$2 \times 2 \times 5\ \mu m^3$	$250 \times 250 \times 1000\ \mu m^3$	$180 \times 180 \times 500\ \mu m^3$	$180 \times 180 \times 500\ \mu m^3$	$200 \times 200 \times 800\ \mu m^3$
T (K)	288[a]	293	293	110	149
Resolution (Å)	1.46	1.4	1.10	1.00	0.82
Refine	REFMAC5	XPLOR	SHELX97 (Sheldrick, 2008)	SHELX97	SHELX97
$\langle B \rangle$ (Å^2)	13.5	11.7	19.4	12.1	11.3
B_{aniso}	yes	no	yes	yes	yes
R_{cryst}/R_{free} (%)	16.5/20.1[b] 11.9/18.1[c]	18.6/22.6	13.3/16.1	13.4/16.1	12.3/14.4
Hydrogen bonds (Å)					
H1: Glu-46	2.54/2.55[d]	2.69	2.58	2.59	2.58
H2: Tyr-42	2.49/2.49[d]	2.71	2.51	2.50	2.48
H3: Cys-69	2.78	2.69	2.82	2.75	2.72

[a]Estimated.
[b]Isotropic B-factor refinement.
[c]Anisotropic B-factor refinement.
[d]long C4'–O4 bond restraints/short C4'–O4 restraints.

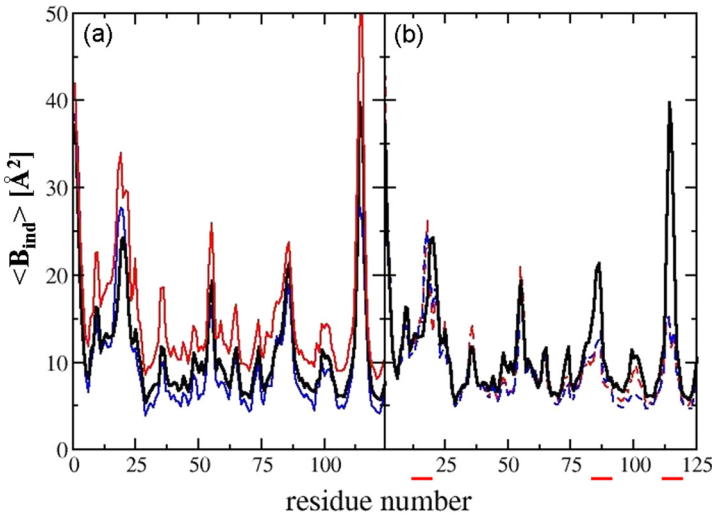

FIG. 5. B-factors averaged over the main chain atoms N, C_α, C, and O and plotted as a function of residue number. (a) B-factors from room temperature structures, black: PYP_{SFX} (1.46 Å), blue: PYP_{B293} (1.4 Å), red: PYP_{A293} (1.10 Å); (b) B-factors in cryo-structures compared to PYP_{SFX} (1.46 Å, thick black line): red: PYP_{A110} (1.10 Å), blue: PYP_{G149} (0.82 Å). Red bars: regions of comparably higher disorder, where the disorder can be partially frozen out.

R_{free} indicates a certain degree of overfitting, which is, however, acceptable in the light of the improved refinement statistics.

In Table II, five different PYP models are compared: PYP_{SFX} (this study), PYP_{B293}, the original model determined by the Getzoff group (Borgstahl *et al.*, 1995), PYP_{A293} and PYP_{A110}, which were both determined at atomic resolution by Anderson and colleagues (Anderson *et al.*, 2004) at room temperature (293 K) and cryogenic temperatures (110 K), respectively, and PYP_{G149} which has been determined to ultra-high resolution (0.82 Å) by Genick and coworkers (Getzoff *et al.*, 2003) at 149 K. Hence, two room temperature structures and two structures determined at cryogenic temperatures are available and can be compared to PYP_{SFX}. PYP_{A293} has the highest overall B-factor, $\langle B \rangle$. To reach 1.1 Å resolution, exposure times to the synchrotron X-rays had to be long. Accordingly, the absorbed X-ray dose is quite high, especially with the relatively small crystals (Table II). Since at room temperature PYP does not show specific local damage (Schmidt, Srajer *et al.*, 2012), the high B-factor reflects global damage. In Fig. 5(a), the temperature factor averaged over individual residue back bone atoms $\langle B \rangle_{ind}$ is plotted as a function of the residue number. The $\langle B \rangle_{ind}$ for the PYP_{A293} (red line) are larger than those for PYP_{SFX} (black line) and PYP_{B293} (blue line). The global damage is revealed by the offset of the red curve with respect to the others. However, for PYP, the global damage does not affect the functionality (the kinetic properties) of the PYP ensemble in the crystal (Schmidt *et al.*, 2012). Despite the potentially higher B-factor, the PYP_{A293} structure is functionally relevant. The smallest B-factor at room temperature is found in the original model PYP_{B293}, which was determined with relatively large crystals and correspondingly low absorbed dose on a home source (Borgstahl *et al.*, 1995). Its $\langle B \rangle$ is as small as those $\langle Bs \rangle$ determined at cryogenic temperatures in PYP_{A110} and PYP_{G149}.

When crystals are frozen, the structural distribution and integrity is maintained even at higher doses (Garman and Weik, 2011; Owen *et al.*, 2006), and resolution as high as 0.82 Å can be reached without noticeable radiation damage. The PYP_{SFX} structure on the other hand shows also low B-values, which are close to the cryogenic structures and the in-house model. This is yet an additional proof that SFX is, due to the "diffraction-before-destruction" principle (Chapman *et al.*, 2011), (almost) free of radiation damage even at room temperature, although doses that are deposited in the tiny crystals may be orders of magnitude higher than the safe dose (Lomb *et al.*, 2011). It can be speculated that the small difference between the $\langle B \rangle$ of the original model PYP_{B293} (Fig. 5(a), blue line) and that of PYP_{SFX} (Fig. 5(a), black line) reflects

some crystal disintegration during the end of the 40 fs X-ray FEL pulse that may be precluded by using even shorter X-ray FEL pulses. The $\langle B \rangle_{ind}$ of the PYP_{SFX} structure are compared to those of the cryogenic structures in Fig. 5(b). The $\langle B \rangle_{ind}$ are almost identical although the structures were determined at different resolutions, at different temperature settings, and from very different crystal sizes. There are notable differences, though, between the cryogenic structures and PYP_{SFX} around residues 16–22, 80–88, and 112–117. All three moieties are loops with little crystal contacts (see Figs. 1 and 5(b), red bars). Their motions can be frozen out by lowering the temperature which increases the Debye Waller factor and the scattering power into the Bragg reflections at low temperatures. The mentioned loop from residue 112–117 might play an important role to mitigate the signal from the chromophore pocket to the periphery of the protein (Ihee *et al.*, 2005; Tenboer *et al.*, 2014).

Hydrogen bonds are important for the functionality of the PYP chromophore (Anderson *et al.*, 2004). They fix the chromophore head between Glu-46 and Tyr-42 (Fig. 3, and Table II). In the original model PYP_{B293}, no unusual hydrogen bond lengths were reported (Table II). The high resolution room and low temperature structures unexpectedly showed that the hydrogen bonds are much shorter (Table II), which supports the idea of a chromophore configuration that is ready to move. Short hydrogen bonds are energetically unfavorable. The chromophore head must be pressed into the hydrogen network due to interactions with amino-acids of the chromophore pocket. Without pocket relaxation the head is tightly kept in position. When a blue photon is absorbed, a *trans* to *cis* isomerization occurs. Since at very early times (100 ps to 1 ns) the pocket relaxations are very limited (Jung *et al.*, 2013; Schotte *et al.*, 2012), the chromophore head cannot move. Instead, the tail rotates (Ihee *et al.*, 2005; Jung *et al.*, 2013; and Schotte *et al.*, 2012). However, when the pocket relaxes at longer times on the μs to ms time-scale (Ihee *et al.*, 2005; Schmidt *et al.*, 2013), the chromophore is ready to snap out of its position. In addition, the putative signaling pB state is very long lived (Schmidt *et al.*, 2013), because the formation of the dark state requires the formation of this tightly knit chromophore pocket. The structural refinement against the SFX data corroborates this view. The hydrogen bonds are short (Table II), irrespective of whether long restraints for the C4'-O4 bond (1.362 Å) or short restraints (1.238 Å) are employed. The hydrogen bonds are much alike to those observed in the highest resolution structures. Moreover, even when the C4'–O4 bond is biased by the short 1.238 Å restraint, it elongates by 0.11 Å to 1.347 Å. This result is also obtained from the highest resolution structures emphasizing again the excellent quality of the SFX data.

Our results show that SFX determines structures in their functional form which are comparable to those determined at both room temperature and cryogenic temperatures at highest resolutions possible. Unlike summarized recently in a review (Schlichting, 2015), the quality of our SFX data is superb. Synchrotron like data quality and resolution are reached at room temperature without suffering from radiation damage. The attenuation mask (Fig. 2(b)) allowed the accurate determination of low resolution intensities without impairing the quality of the high resolution data. Furthermore, the CSPAD tile geometry (Fig. 2(b)) can be exquisitely well determined by refining individual tile positions with help of the X-ray data (Tenboer *et al.*, 2014). All of this resulted in highly accurate amplitudes even in the presence of an indexing ambiguity and without introducing partiality models (Kabsch, 2014; Sauter *et al.*, 2013). For the collection of the $\sim 2.5 \times 10^6$ snapshots, about 6 h of FEL beamtime is necessary. With an average jet flow of 22 μl/min, about 7.6 ml of crystal slurry is dissipated which contains roughly 500 mg of microcrystalline protein. It is desirable, therefore, to reduce the number of required X-ray snapshots with computational methods (Sauter, 2015; Uervirojnangkoorn *et al.*, 2015; and White, 2014) to obtain comparable data quality within much shorter beamtimes, collecting a much smaller number of snapshots from a much lower amount of protein.

SUMMARY

We push the resolution of macromolecular serial femtosecond crystallography to 1.46 Å. Anisotropic B-factor refinement starts to become possible with SFX data at that resolution. The

structures show little to no evidence of radiation damage even at ambient temperatures and are comparable to ultrahigh (atomic) resolution structures.

ACKNOWLEDGMENTS

This work was supported by NSF-STC "Biology with X-ray Lasers" (NSF-1231306). M.S. was also supported by NSF-0952643 (Career). Shibom Basu was supported by NIH Grant No. R01GM095583 (to Petra Fromme). Kanupriya Pande was supported by NSF-1158138 (to Dilano Saldin and Marius Schmidt).

Anderson, S., Crosson, S., and Moffat, K., "Short hydrogen bonds in photoactive yellow protein," Acta Crystallogr. D **60**, 1008–1016 (2004).
Barty, A., Kirian, R. A., Maia, F. R. N. C., Hantke, M., Yoon, C. H., White, T. A., and Chapman, H., "Cheetah: Software for high-throughput reduction and analysis of serial femtosecond X-ray diffraction data," J. Appl. Crystallogr. **47**, 1118–1131 (2014).
Berman, H. M., Battistuz, T., Bhat, T. N., Bluhm, W. F., Bourne, P. E., Burkhardt, K., and Zardecki, C., "The protein data bank," Acta Crystallogr. D **58**(Pt 6 No 1), 899–907 (2002).
Borgstahl, G. E., Williams, D. R., and Getzoff, E. D., "1.4 A structure of photoactive yellow protein, a cytosolic photoreceptor: Unusual fold, active site, and chromophore," Biochemistry **34**(19), 6278–6287 (1995).
Brehm, W. and Diederichs, K., "Breaking the indexing ambiguity in serial crystallography," Acta Crystallogr. D **70**(Pt 1), 101–109 (2014).
Brown, A., Long, F., Nicholls, R. A., Toots, J., Emsley, P., and Murshudov, G., "Tools for macromolecular model building and refinement into electron cryo-microscopy reconstructions," Acta Crystallogr. D **71**, 136–153 (2015).
Brunger, A. T., Adams, P. D., Clore, G. M., DeLano, W. L., Gros, P., Grosse-Kunstleve, R. W., and Warren, G. L., "Crystallography & NMR system: A new software suite for macromolecular structure determination," Acta Crystallogr. D **54**(Pt 5), 905–921 (1998).
Brunger, A. T., Krukowski, A., and Erickson, J. W., "Slow-cooling protocols for crystallographic refinement by simulated annealing," Acta Crystallogr A **46**(Pt 7), 585–593 (1990).
Chapman, H. N., Fromme, P., Barty, A., White, T. A., Kirian, R. A., Aquila, A., and Spence, J. C., "Femtosecond X-ray protein nanocrystallography," Nature **470**(7332), 73–77 (2011).
DeLano, W. L., *The Pymol Molecular Graphics System* (DeLano Scientific LLC, San Carlos, CA, 2006).
Emsley, P., Lohkamp, B., Scott, W. G., and Cowtan, K., "Features and development of Coot," Acta Crystallogr. D **66**(Pt 4), 486–501 (2010).
Garman, E. F. and Weik, M., "Macromolecular crystallography radiation damage research: What's new?," J. Synchrotron Radiat. **18**, 313–317 (2011).
Getzoff, E. D., Gutwin, K. N., and Genick, U. K., "Anticipatory active–site motions and chromophore distortion prime photoreceptor PYP for light activation," Nat. Struct. Biol. **10**(8), 663–668 (2003).
Ihee, H., Rajagopal, S., Srajer, V., Pahl, R., Anderson, S., Schmidt, M., and Moffat, K., "Visualizing reaction pathways in photoactive yellow protein from nanoseconds to seconds," Proc. Natl. Acad. Sci. U.S.A. **102**(20), 7145–7150 (2005).
Jung, Y. O., Lee, J. H., Kim, J., Schmidt, M., Moffat, K., Srajer, V., and Ihee, H., "Volume-conserving trans-cis isomerization pathways in photoactive yellow protein visualized by picosecond X-ray crystallography," Nat. Chem. **5**(3), 212–220 (2013).
Kabsch, W., "Processing of X-ray snapshots from crystals in random orientations," Acta Crystallogr D **70**(Pt 8), 2204–2216 (2014).
Karplus, P. A. and Diederichs, K., "Linking crystallographic model and data quality," Science **336**(6084), 1030–1033 (2012).
Kleywegt, G. J., Zou, J. Y., Kjeldgaard, M., and Jones, A., *International Tables for Crystallography*, Vol. F, pp. 353–356 (Kluwer Academic Publishers, Dordrecht, 2001).
Lomb, L., Barends, T. R., Kassemeyer, S., Aquila, A., Epp, S. W., Erk, B., and Schlichting, I., "Radiation damage in protein serial femtosecond crystallography using an x-ray free-electron laser," Phys. Rev. B **84**(21), 214111 (2011).
Meyer, T. E., "Isolation and characterization of soluble cytochromes, ferredoxins and other chromophoric proteins from the halophilic phototrophic bacterium Ectothiorhodospira halophila," Biochim. Biophys. Acta **806**(1), 175–183 (1985).
Murshudov, G. N., Skubak, P., Lebedev, A. A., Pannu, N. S., Steiner, R. A., Nicholls, R. A., and Vagin, A. A., "REFMAC5 for the refinement of macromolecular crystal structures," Acta Crystallogr. D **67**(Pt 4), 355–367 (2011).
Owen, R. L., Rudino-Pinera, E., and Garman, E. F., "Experimental determination of the radiation dose limit for cryocooled protein crystals," Proc. Natl. Acad. Sci. U.S.A. **103**(13), 4912–4917 (2006).
Pettersen, E. F., Goddard, T. D., Huang, C. C., Couch, G. S., Greenblatt, D. M., Meng, E. C., and Ferrin, T. E., "UCSF chimera—A visualization system for exploratory research and analysis," J. Comput. Chem. **25**(13), 1605–1612 (2004).
Sauter, N. K., "XFEL diffraction: Developing processing methods to optimize data quality," J. Synchrotron Radiat. **22**, 239–248 (2015).
Sauter, N. K., Hattne, J., Grosse-Kunstleve, R. W., and Echols, N., "New Python-based methods for data processing," Acta Crystallogr. D **69**(Pt 7), 1274–1282 (2013).
Scheres, S. H. W., "RELION: Implementation of a Bayesian approach to cryo-EM structure determination," J. Struct. Biol. **180**(3), 519–530 (2012).
Schlichting, I., "Serial femtosecond crystallography: The first five years," IUCrJ **2**, 246–255 (2015).
Schmidt, M., Pahl, R., Srajer, V., Anderson, S., Ren, Z., Ihee, H., and Moffat, K., "Protein kinetics: Structures of intermediates and reaction mechanism from time-resolved x-ray data," Proc. Natl. Acad. Sci. U.S.A. **101**(14), 4799–4804 (2004).
Schmidt, M., Srajer, V., Henning, R., Ihee, H., Purwar, N., Tenboer, J., and Tripathi, S., "Protein energy landscapes determined by five-dimensional crystallography," Acta Crystallogr. D **69**, 2534–2542 (2013).

Schmidt, M., Srajer, V., Purwar, N., and Tripathi, S., "The kinetic dose limit in room-temperature time-resolved macromolecular crystallography," J. Synchrotron Radiat. **19**(Pt 2), 264–273 (2012).
Schotte, F., Cho, H. S., Kaila, V. R., Kamikubo, H., Dashdorj, N., Henry, E. R., and Anfinrud, P. A., "Watching a signaling protein function in real time via 100-ps time-resolved Laue crystallography," Proc. Natl. Acad. Sci. U.S.A. **109**(47), 19256–19261 (2012).
Sheldrick, G. M., "A short history of SHELX," Acta Crystallogr. A **64**(Pt 1), 112–122 (2008).
Tenboer, J., Basu, S., Zatsepin, N., Pande, K., Milathianaki, D., Frank, M., and Schmidt, M., "Time-resolved serial crystallography captures high-resolution intermediates of photoactive yellow protein," Science **346**(6214), 1242–1246 (2014).
Uervirojnangkoorn, M., Zeldin, O. B., Lyubimov, A. Y., Hattne, J., Brewster, A. S., Sauter, N. K., and Weis, W. I., "Enabling X-ray free electron laser crystallography for challenging biological systems from a limited number of crystals," Elife **4**, e05421 (2015).
Weierstall, U., Spence, J. C., and Doak, R. B., "Injector for scattering measurements on fully solvated biospecies," Rev. Sci. Instrum. **83**(3), 035108 (2012).
White, T. A., "Post-refinement method for snapshot serial crystallography," Philos. Trans. R. Soc. B **369**(1647), 20130330 (2014).
White, T. A., Kirian, R. A., Martin, A. V., Aquila, A., Nass, K., Barty, A., and Chapman, H. N., "CrystFEL: A software suite for snapshot serial crystallography," J. Appl. Crystallogr. **45**, 335–341 (2012).